Synthesis and electrical properties of $Pb(Mg_{1/3}Nb_{2/3})O_3$-$PbTiO_3$ epitaxial thin films on Si wafers using chemical solution deposition

Takashi Arai, Tomoya Ohno, Takeshi Matsuda, Naonori Sakamoto, Naoki Wakiya, Hisao Suzuki

PII: S0040-6090(16)00080-8
DOI: doi: 10.1016/j.tsf.2016.01.058
Reference: TSF 34998

To appear in: *Thin Solid Films*

Received date: 1 December 2015
Revised date: 26 January 2016
Accepted date: 30 January 2016

Please cite this article as: Takashi Arai, Tomoya Ohno, Takeshi Matsuda, Naonori Sakamoto, Naoki Wakiya, Hisao Suzuki, Synthesis and electrical properties of $Pb(Mg_{1/3}Nb_{2/3})O_3$-$PbTiO_3$ epitaxial thin films on Si wafers using chemical solution deposition, *Thin Solid Films* (2016), doi: 10.1016/j.tsf.2016.01.058

Synthesis and electrical properties of $Pb(Mg_{1/3}Nb_{2/3})O_3$-$PbTiO_3$ epitaxial thin films on Si wafers using chemical solution deposition

Takashi Arai[a], Tomoya Ohno[b], Takeshi Matsuda[b], Naonori Sakamoto[c], Naoki Wakiya[c], and Hisao Suzuki[c]

[a] Graduate School of Science and Technology, Shizuoka University

3-5-1 Johoku, Hamamatsu, Shizuoka, Japan 432-8561

[b] Department of Materials Science, Kitami Institute of Technology

165 Kouen-cho, Kitami, Japan 090-8507

[c] Research Institute of Electronics, Shizuoka University,

3-5-1 Johoku, Hamamatsu, Shizuoka, Japan 432-8561

Corresponding author

Takashi Arai

arai.takashi.14@shizuoka.ac.jp

TEL&FAX: +81-053-478-1157

Abstract

$Pb(Mg_{1/3}Nb_{2/3})O_3$-$PbTiO_3$ (PMN-PT) has attracted a great deal of attention for its use in capacitors, piezoelectric actuators, sensors, and optical devices in integrated circuits. For these applications, epitaxially grown PMN-PT thin films on Si wafers are required. This paper describes the first trial in fabricating epitaxially grown PMN-PT thin films on a LSCO/CeO_2/YSZ buffered Si substrate using chemical solution deposition (CSD). High quality buffer layers make the epitaxial growth of PMN-PT thin films possible, even by CSD. Despite very thin films that have thicknesses of 170 nm, the resulting PMN-PT thin films exhibit good electrical properties, such as a high dielectric constant of 1400 and well-defined P-E hysteresis loops.

1. Introduction

Solid solutions consisting of lead magnesium niobate and lead titanate, i.e., (1-x)Pb($Mg_{1/3}Nb_{2/3}$)O_3-x$PbTiO_3$ (PMN-PT), are well known as relaxor-based perovskite-type ferroelectrics with superior electrical properties, such as high dielectricity ($\varepsilon_{33}^T/\varepsilon_0$=8200), giant piezoelectricity (d_{33}=2800 pC/N), and excellent electromechanical coupling coefficient (k_{33}=94%) [1]. These electrical properties show maximum peaks at the morphotropic phase boundary (MPB) around a composition of *x* = 0.35 at room temperature [2]. Therefore, PMN-PT ferroelectrics with a MPB composition have attracted much attention as potential applications in many advanced devices, such as piezoelectric actuators, sensors, energy-harvesting devices, and electro-optic devices.

Recently, many advanced thin films, including ferroelectric thin films, have been increasingly used in integrated circuits (ICs). For IC technologies, the Si substrate is essential, and suitable thin film deposition techniques, such as chemical solution deposition (CSD) [3-8], sputtering [9,10], and pulsed laser deposition (PLD) [11], have been modified to enhance the compatibility with the IC technology. Therefore, in this paper, the epitaxial growth of PMN-PT thin films is investigated on a Si wafer using high quality buffer layers to allow for the compatibility with the IC technology. To date,

arbitrarily or uniaxially oriented PMN-PT thin films grown on Si substrates have been established and reported. Epitaxially grown thin films are generally regarded as ideal structures for exhibiting high electrical properties, reliability of devices, and high stability of properties [12]. Nevertheless, it is difficult to realize the epitaxial growth of ferroelectric thin films on Si substrates because of the unavoidable presence of a SiO_x layer. Several attempts have been made to grow epitaxial thin films by introducing special buffer layers, such as $La(Sr,Co)O_3$ (LSCO)/CeO_2/YSZ [13], $SrRuO_3$ (SRO)/$SrTiO_3$ (STO) [14], SRO/STO/TiN [15], MgO/TiN [16], LSCO/STO [17], and $MgAl_2O_4$ [18] on Si substrates using PLD. Furthermore, the modification of a suitable deposition technique is extremely important for the deposition of epitaxial PMN-PT thin films with high stability and desirable properties. Physical vapor deposition techniques (PVD), such as PLD, have been used for the growth of epitaxial PMN-PT (perovskite-type) thin films on $SrTiO_3$, MgO single crystals, and even on Si substrates. However, these PVD techniques have resulted in the formation of an undesired pyrochlore phase and a high leakage current because of defect formation during deposition. Furthermore, compositional adjustments in the films, while allowing for repeatability with the desired phase, is still challenging for PVD techniques. In contrast, using CSD, it is easy to control the composition from the molecular designed precursor

solutions. To the best of our knowledge, no reports in the relevant literature have described the fabrication of epitaxial PMN-PT thin films on a Si wafer using CSD.

Our previous report described the growth of CSD-derived uniaxially oriented PMN-PT thin films deposited on a Si substrate at low temperatures, which showed good electrical properties. In the previous paper, the importance of the amount of excess Pb in the precursor solution was stressed, as well as the sintering conditions of the as-deposited thin films [19]. In reality, excess Pb should be added to the precursor solutions to compensate for its loss during the heat treatment because Pb can easily volatilize upon heating. Moreover, Pb deficiency leads to the formation of the pyrochlore phase and/or atomic defects, which can reduce the electrical properties of the resulting PMN-PT films. However, too much excess Pb induces the formation of a residual Pb excess phase, which may diffuse into the Si substrate, leading to reduced and unstable electrical properties even in the case of ceramics [20,21].

Therefore, this paper is aimed at investigating the suitable amount of excess Pb in the precursor solution for obtaining better electrical properties of the CSD-derived epitaxial PMN-PT thin films on Si substrates. For the perovskite-type epitaxially grown thin films, LSCO/CeO_2/YSZ buffer layers have been introduced between the Si substrate and the PMN-PT thin film using PLD [13]. Few materials can grow epitaxially on Si

because of the very thin amorphous SiO_2 layer on the surface of Si. Therefore, we introduce a thin YSZ buffer layer on Si because YSZ is one of the materials known to grow epitaxially on Si with thin SiO_2 layer [13]. However, it is known that perovskite materials cannot grow epitaxially on YSZ. Therefore, CeO_2 is introduced as a buffer layer for the epitaxial growth of perovskite materials on YSZ. LSCO can act as not only a buffer layer for the epitaxial growth of PMN-PT but also as a bottom electrode. Subsequently, the electrical properties of the resulting PMN-PT films are compared with that of PMN-PT films reported elsewhere.

2. Experimental procedures

The starting reagents for the PMN-PT precursor solution with a MPB composition of x=0.35 were lead acetate trihydrate [$Pb(OCOCH_3)_2 \cdot 3H_2O$], titanium isopropoxide [$Ti(i\text{-}OC_3H_7)_4$], magnesium ethoxide [$Mg(OC_2H_5)_2$], and niobium ethoxide [$Nb(OC_2H_5)_5$]. The solvent used in this study was ethanol. To remove crystalline water, $Pb(OCOCH_3)_2 \cdot 3H_2O$ was dried at 150 °C for 2 h, followed by refluxing with NH_3 flow in ethanol for 2 h at 50 °C. Excess lead source (0, 5, 10, 15, 20, 25, and 30 mol% excess) was added to the precursor solutions to compensate for the loss of lead by volatilization and diffusion into the electrode during heating, although the addition of

too much excess lead will result in residual lead oxide. Therefore, in this study, the suitable amount of excess lead was optimized by measuring the electrical properties of the resultant thin films. Then, the sources of the B-site cations of the perovskite structure, i.e., $Ti(i\text{-}OC_3H_7)_4$, $Mg(OC_2H_5)_2$, and $Nb(OC_2H_5)_5$, were refluxed in ethanol for 4 h at 78 °C because the Columbite method is effective in suppressing the formation of the pyrochlore phase in the case of bulk ceramics [22]. These solutions were mixed and reacted for 2 h at 78 °C. Finally, 2-aminoethanol was added to stabilize the obtained precursor solutions. The concentration of the precursor solutions was adjusted to be 0.1 M.

LSCO/CeO_2/YSZ buffer layers were deposited by PLD. Details of the LSCO/CeO_2/YSZ buffer layer deposition have already been reported elsewhere [13].

The PMN-PT layers were deposited repeatedly on the LSCO/CeO_2/YSZ/Si substrate by spin coating to increase the film thickness up to 170 nm. The as-deposited PMN-PT layer was dried at 150 °C for 10 min and pre-annealed at 450 °C for 10 min. Lastly, the films were annealed at 650 °C for 5 min, which was the optimum crystallization temperature for this precursor [19].

The crystal structure was identified using X-ray diffraction (XRD, D8 Advance; Bruker Corp.) using θ–2θ scan with Cu Kα radiation and a scan speed of 3.3 deg/min.

Dielectricity was measured using an impedance analyzer (HP; 4194A) at 1 kHz. Ferroelectricity was evaluated using a ferroelectric test system (FCE-PZ type; Toyo Technica Inc.) at 1 kHz. Both Φ-scan and ω-scan were measured using an advanced thin film X-ray grazing-system (ATX-G; Rigaku Corp.) with Cu Kα radiation. The thin film microstructure, electron diffraction pattern, and energy dispersive X-ray spectrometry (EDS) were observed using transmission electron microscopy (TEM, JEM-2001F; JEOL) with an operating voltage of 200 kV. The local piezoelectric response was observed using an atomic force microscope (AFM, SPI3800N; SII Nano Technology Inc.) equipped with a piezoelectric force mode. A Rh-coated Si tip with a resonance frequency of approx. 129 kHz (14 N/m tip stiffness) was used for these measurements (Hitachi High-Tech Science Corp.). An electric field (±10 V, 60 Hz) was applied between the top Pt electrode with a diameter of 50 μm on the PMN-PT surface and the LSCO bottom electrode of the thin film to observe the local displacement induced electric field. Each measurement was taken at room temperature.

3. Results

3.1. Identification of the crystal phase and optimization of the lead content

Fig. 1 presents the XRD θ–2θ pattern for PMN-PT/LSCO/CeO_2/YSZ/Si thin films with different excess Pb contents from 0–30 mol% in the precursor solutions. All PMN-PT thin films grown on the LSCO/CeO_2/YSZ/Si substrate exhibited a single-phase (100)-oriented perovskite structure independent of the amount of excess Pb content. These results suggested that the (100)-oriented LSCO bottom electrode acted as a seeding layer to control the orientation of the resulting PMN-PT thin films and suppressed the pyrochlore phase formation effectively. The reported crystallization temperature for CSD-derived PMN-PT thin films was higher than 800 °C (Table 1). However, these thin films were crystallized to the (100)-oriented perovskite structure at lower temperatures because of the molecule designed-precursor solution and the (100)-oriented perovskite-type LSCO bottom electrode.

Fig. 2 presents the dielectric constants and dielectric loss for the PMN-PT thin films on LSCO/CeO_2/YSZ/Si substrates measured at a frequency of 1 kHz and at room temperature as a function of the excess lead content in the precursor solution. The dielectric constants and the dielectric loss were observed to be almost constant, i.e., at 1400 and 0.06, respectively, for films grown from 0–20 mol% of excess lead content in the precursor. However, the films prepared with an excess Pb content greater than 20 mol% exhibited an increment in the dielectric constant, as well as the dielectric loss, as

a function of to the excess Pb mol%. This increment can be attributed to the increase of remnant lead in the resultant films, which formed a residual Pb excess phase. The absence of its reflection in the XRD measurement was ascribed to a lower crystallinity or lower content of the secondary phase. This increase in the dielectric loss was also ascribed to lead diffusion into the substrate during the annealing process (650°C). Therefore, the analysis of elemental diffusion for the resultant films is described in the next section.

Fig. 3 demonstrates the P–E hysteresis loops of PMN-PT thin films grown on LSCO/CeO_2/YSZ/Si substrates measured at room temperature and 1 kHz as a function of excess Pb mol%. In Fig. 3, it is readily apparent that the PMN-PT thin films with an excess Pb content above 20 mol% in the precursor solution exhibited saturated and well-defined P–E hysteresis loops even under high electric fields (860 kV/cm). Leaky loops were observed for films grown with precursor contents of less than 20 mol% excess lead. This leakage can be ascribed to the formation of defect centers in the PMN-PT thin films prepared with lower (<20 mol%) excess Pb content in the precursor solution, which probably caused a Pb deficiency in the films. The shortage of lead in the films may be attributed to lead volatilization during heat treatment. Therefore, leakage in the current appeared in the P–E loops when high electric fields were applied.

Based on these results, we concluded that the optimum amount of excess Pb % added to the precursor for the growth of perovskite type PMN-PT thin films with better electrical properties was between 15–20 mol%. This result was attributed to the avoidance of negative effects caused by the lead excess phase and lead deficiency, which significantly affected the electrical properties of PMN-PT thin films on Si substrates.

Furthermore, these thin films with thicknesses of 170 nm prepared from the precursor solution with an excess lead content of 20 mol% exhibited superior electrical properties, with good mean values of the dielectric constant (ε: 1438), dielectric loss (tanδ : 0.051), and remnant polarization (P_r : 9.1 uC/cm^2). These observations agreed closely with those of epitaxially grown PMN-PT thin films deposited by PLD (Table 1). However, measuring the electrical properties of a ferroelectric material with a thickness of approx. 100 nm is difficult. As reported, we successfully grew high-quality PMN-PT thin films with thicknesses of 170 nm with good electrical properties despite of the low sintering temperature. Comprehensive results are listed in Table 1.

3.2. Epitaxial growth

The structural analysis of CSD-derived PMN-PT thin films with excess lead contents

of 15–20 mol% on LSCO/CeO_2/YSZ/Si substrates was conducted using several analytical methods.

To confirm the epitaxial growth and the in-plane orientation for the PMN-PT thin films on a LSCO/CeO_2/YSZ/Si substrate, XRD Φ-scan measurements were carried out for the PMN-PT thin films. Fig. 4 displays the typical Φ-scan results of PMN-PT (101) and LSCO (101), as well as Si (202). Four diffraction peaks were observed for each PMN-PT, LSCO, and Si layer and were rotated by 90 degrees, which represented the four-folded symmetry of PMN-PT, LSCO, and Si. The diffraction peaks of PMN-PT and LSCO were at the same Φ-position, which indicated the epitaxial growth of PMN-PT thin films with a cube-on-cube relation on the (100) surface of the LSCO bottom electrode. On the other hand, the diffraction peaks of LSCO were located on Si with a 45 degree rotation. This result showed good agreement with that presented in previous reports [13], i.e., YSZ and CeO_2 layers were grown heteroepitaxially on a Si (100) substrate with a cube-on-cube relation; on CeO_2 thin films, LSCO and PMN thin films were grown heteroepitaxially with a 45 degree rotated relation. These results confirmed that CSD-derived PMN-PT thin films were grown epitaxially on a Si substrate using sophisticated buffer layers with PLD.

The out-of-plane crystallinity was examined by a rocking curve (ω-scan) of the

PMN-PT (200) diffraction peak, as presented in Fig. 5. The full width at half maximum (FWHM) of the rocking curve was 0.57°. This value was relatively narrow compared to that reported elsewhere in the literature [8, 15, 23, 24, 25]. The narrowness of the rocking curves of the PMN-PT films indicated a high degree of oriented growth and excellent crystallinity. This result was attributed purely to the superior in-plane lattice matching of the very thin PMN-PT film with the LSCO bottom electrode layer.

The surface morphologies of the epitaxial PMN-PT thin film on the LSCO electrode and LSCO on the CeO_2/YSZ/Si template were examined using AFM measurements. Fig. 6 presents AFM images for (a) the LSCO surface of the LSCO/CeO_2/YSZ/Si substrate and (b) the PMN-PT surface on LSCO/CeO_2/YSZ/Si substrates. The surface roughness values (RMS) of both surfaces were approx. 2 nm, demonstrating a very smooth growth of PMN-PT and LSCO films on LSCO/CeO_2/YSZ/Si and CeO_2/YSZ/Si multilayered templates, respectively. This value was lower than the reported value (6.1 nm) [23] of a 300-nm-thick PLD-derived PMN-PT thin film grown on the same buffer layer. These observations indicated that CSD was a suitable method for the deposition of single-phase perovskite type PMN-PT thin films with smooth surface roughness.

Cross-sectional TEM measurements were conducted on the PMN-PT/LSCO/CeO_2/YSZ/Si heterostructured thin film. Fig. 7(a) shows its

cross-sectional bright field TEM micrograph from which the thickness of each layer was estimated for the PMN-PT/LSCO/CeO_2/YSZ multilayers on Si. The measured thicknesses of the PMN-PT, LSCO, CeO_2, and YSZ individual layers were 170, 30, 35, and 20 nm, respectively. No marked inter-diffusion was detected between PMN-PT and the LSCO bottom electrode.

Selected area electron diffraction measurements further confirmed the epitaxial growth of PMN-PT thin films. Fig. 7(b) portrays the electron diffraction pattern for the cross-sectional PMN-PT thin film deposited on a LSCO/CeO_2/YSZ/Si substrate. The 00l spots from PMN-PT were observed in the in-plane direction, and the h00 spots from PMN-PT were observed in the out-of-plane direction. In the in-plane direction, the hh0 spots of the Si substrate and 00h spots of PMN-PT corresponded mutually. These observations were congruent with the XRD Φ-scan measurements, confirming the epitaxial growth of PMN-PT thin films on Si substrates.

Elemental diffusion analysis was used to elucidate the phase evolution and the interface of the samples. STEM–EDS analysis was used for a PMN-PT/LSCO/ CeO_2/YSZ/Si sample to obtain the elemental depth profile. Then, Pb, Co, Ce, Zr, and Si atoms were measured to investigate their distributions. The results are presented in Fig. 8. In many cases of Pb-based thin films, diffusion of Pb towards the substrate was

reported [26]. However, elemental diffusion was not observed in our thin films. The presence of a Si peak signature in the other layers might be attributed to a partial overlap between the detected energies of the other elements. Therefore, the reacted phase between lead and the other elements could be ignored in the discussion of the electrical properties.

3.3 Factors affecting the piezoelectric properties of PMN-PT thin films

The effective piezoelectric constants (d_{33}^{eff}) for epitaxially grown PMN-PT thin films on a single crystal substrate, such as STO, have been reported [27, 28]. To date, however, no report in the literature has described a study on the piezoelectric properties of CSD-derived PMN-PT epitaxial thin films grown on versatile Si substrates. Fig. 9 presents the typical piezoelectric response of CSD-derived epitaxially grown PMN-PT thin films on a Si substrate. In this study, the displacement of PMN-PT thin film on a LSCO/CeO_2/YSZ/Si substrate was estimated as 200 pm at an applied voltage of 10 V, meaning that d_{33}^{eff} was calculated to be 20 pm/V. This smaller d_{33}^{eff} of 20 pm/V compared to that reported elsewhere [9,19,27,28,29] should be ascribed to the negative effect of the residual stress. When the PMN-PT thin film (thermal expansion coefficient, TEC: 6.3×10^{-6}/K [30]) was deposited on a Si substrate with low TEC (2.6×10^{-6}/K [31]),

tensile stress should remain in the resulting PMN-PT thin films, which arose from the Si substrate during cooling. On the other hand, compressive stress was expected to remain in PMN-PT when PMN-PT was deposited on substrates with large TECs, such as MgO (TEC: 8×10^{-6}/K [32]) or STO (TEC: 9×10^{-6}/K [33]), to exhibit their higher piezoelectricity. Han et al. reported that when PZT thin films were deposited on Si wafers, tensile stress was applied to the PZT thin films, leading to a lower d_{33}^{eff} and remnant polarization (P_r) [34]. From these results, we can assume the existence of tensile stress in the epitaxially grown PMN-PT thin films on Si substrates. On the other hand, for PMN-PT thin films deposited on a Si substrate, remnant polarizations have been reported to be around P_r =7 uC/cm^2 [3,9,23]. Our thin film showed a higher P_r value of 9.1 uC/cm^2 because of the high crystallinity or small FWHM as shown in Fig. 5, despite the very thin thickness of the film. This can be confirmed from the results of previous research, in which P_r exhibited over a value of 10 uC/cm^2 [24,25,29,36] for PMN-PT thin films deposited on substrates with large thermal expansion coefficients because compressive stress remained in these films. Therefore, we concluded that the epitaxial PMN-PT thin film deposited in this study could be tensile, leading to the lower d_{33}^{eff}. To increase this value, we can control the residual stress in the ferroelectric thin films on the Si wafer. We already reported the control of stress in PMN-PT thin films

using porous $LaNiO_3$ layers, leading to a much higher d_{33}^{eff} [19]. Although d_{33}^{eff} in this study was smaller than those of the previous films, we can expect the presence of other superior properties, such as optical and electro-optical effects, for the epitaxially grown PMN-PT thin film on a Si substrate using CSD because of the very thin thickness and high crystallinity. In this work, we successfully demonstrated that very thin epitaxially grown PMN-PT films could be deposited even on a Si substrate if a high quality buffer layer was suitably inserted between the ferroelectric thin film and the substrate.

4. Conclusion

This paper described the first investigations of CSD-derived epitaxially grown PMN-PT thin films on a Si substrate using PLD-derived LSCO/CeO_2/YSZ buffer layers. The electrical properties of CSD-derived PMN-PT thin films were strongly affected by the excess lead contents in the precursor solution. These films exhibited superior electrical properties, i.e., dielectric constant (average ε: 1438), dielectric loss (average tanδ: 0.051), and remnant polarization (average $P_{r:}$ 9.1 uC/cm^2), despite their very thin film thickness of 170 nm and low sintering temperature of 650 °C. Furthermore, the piezoelectric response of the film was measured as d_{33}^{eff} =20 pm/V. Although d_{33}^{eff} was smaller than that reported previously because of the residual tensile stress in the film,

the epitaxial PMN-PT thin film can be applied in optical and electro-optic devices due to its high crystallinity and very thin film thickness.

Figure captions

Figure 1. XRD θ–2θ patterns for PMN-PT/LSCO/CeO_2/YSZ/Si thin films.

Figure 2. Dielectric constants and dielectric loss for PMN-PT thin films on LSCO/CeO_2/YSZ/Si at room temperature and 1 kHz as a function of the lead content.

Figure 3. P–E hysteresis loops for PMN-PT thin films on LSCO/CeO_2/YSZ/Si with various lead contents at room temperature and 1 kHz.

Figure 4 XRD Φ-scan for Si (202), LSCO (101), and PMN-PT (101) of PMN-PT/LSCO/CeO_2/YSZ/Si.

Figure 5. Rocking curve (ω-scan) for PMN-PT (002) of PMN-PT/LSCO/CeO_2/YSZ/Si.

Figure 6. AFM images for (a) LSCO surface of the LSCO/CeO_2/YSZ/Si substrate and (b) PMN-PT surface on LSCO/CeO_2/YSZ/Si.

Figure 7. (a) Cross-sectional bright field image and (b) electron diffraction pattern of PMN-PT/LSCO/CeO_2/YSZ/Si from TEM.

Figure 8. Line profiles for the main elements in the PMN-PT films on LSCO/CeO_2/YSZ/Si from STEM-EDS.

Figure 9. Piezoelectric response of epitaxially grown PMN-PT thin films on Si substrates.

Table title

Table 1. Electrical properties of PMN-PT thin films with a MPB composition deposited by different methods on different substrates reported in the literature

Acknowledgements

Part of this work was supported by Concert-Japan Project (FF-Photon) from Japan Science and Technology Agency.

References

[1] R. Zhang, B. Jiang, W. Cao, Elastic, piezoelectric, and dielectric properties of multidomain 0.67Pb($Mg_{1/3}Nb_{2/3}$)O_3-0.33$PbTiO_3$ single crystals, J. Appl. Phys. 90 (2001) 3471–3475.

[2] T.Y. Koo, S-W. Cheong, Dielectric and piezoelectric enhancement due to 90° domain rotation in the tetragonal phase of Pb($Mg_{1/3}Nb_{2/3}$)O_3-$PbTiO_3$, Appl. Phys. Lett. 80 (2002) 4205–4207.

[3] M.-J. Shyu, T.-J. Hong, T.-J. Yang, T.-B. Wu, Highly (100)-Oriented Thin Films of Sol--gel Derived Pb[($Mg_{1/3}Nb_{2/3}$)$_{0.675}Ti_{0.325}$]O_3 Prepared on Textured $LaNiO_3$ Electrode, Jpn. J. Appl. Phys. 34 (1995) 3647–3653.

[4] W. Gong, J.-F. Li, X. Chu, L. Li, Texture Control of Sol–Gel Derived Pb($Mg_{1/3}Nb_{2/3}$)O_3-$PbTiO_3$ Thin Films Using Seeding Layer, J. Am. Ceram. Soc. 87 (2004) 1031–1034.

[5] M.L. Calzada, M. Alguero, J. Ricote, A. Santos, L. Pardo, Preliminary results on sol–gel processing of <100> oriented Pb($Mg_{1/3}Nb_{2/3}$)O_3-$PbTiO_3$ thin films using diol-based solutions, J. Sol–gel Sci. Techn. 42 (2007) 331–336.

[6] S.A. Yang, S.Y. Cho, J.S. Lim, S.D. Bu, Distribution of pyrochlore phase in $Pb(Mg_{1/3}Nb_{2/3})O_3$-$PbTiO_3$ films and suppression with a $Pb(Zr_{0.52}Ti_{0.48})O_3$ interfacial layer, Thin Solid Films 520 (2012) 7071–7075.

[7] Y. Bastani, N. Bassiri-Gharb, Processing Optimization of Lead Magnesium Niobate-Lead Titanate Thin Films for Piezoelectric MEMS Application, J. Am. Ceram. Soc. 95 [4] (2012) 1269–1275.

[8] J. Hwan Park, F. Xu, S. Trolier-McKinstry, Dielectric and piezoelectric properties of sol–gel derived lead magnesium niobium titanate films with different textures, Journal of Applied Physics 89 (2001) 568–574.

[9] M. Detallea, G. Wanga, D. Re´miensa, P. Ruterana, P. Roussel, B. Dkhil, Comparison of structural and electrical properties of PMN-PT films deposited on Si with different bottom electrodes, J. Crystal Growth 305 (2007) 137–143.

[10] Z. Feng, D. Shi, R. Zeng, S. Dou, Large electrocaloric effect of highly (100)-oriented $0.68PbMg_{1/3}Nb_{2/3}O_3$–$0.32PbTiO_3$ thin films with a $Pb(Zr_{0.3}Ti_{0.7})O_3/PbO_x$ buffer layer, Thin Solid Films 519 (2011) 5433–5436.

[11] X.Y. Chen, J. Wang, K.H. Wong, C.L. Mak, G.X. Chen, J.M. Liu, M. Wang, Z.G. Liu, Growth of orientation-controlled $Pb(Mg_{1/3}Nb_{2/3})O_3$-$PbTiO_3$ thin films on

Si(100) by using oriented MgO films as buffers, Appl. Phys. A 81 (2005) 1145–1149.

[12] R. Ramesh, D.G. Schlom, Orienting Ferroelectric Films, Science 296 (2002) 1975–1976.

[13] N. Wakiya, K. Shinozaki, N. Mizutani, Preparation of heteroepitaxial $Pb(Mg_{1/3}Nb_{2/3})O_3$ (PMN) thin film by pulsed laser deposition on Si(001) substrate using $La_{0.5}Sr_{0.5}CoO_3$ (LSCO)/CeO_2/YSZ triple buffer, Thin Solid Films 384 (2001) 189–194.

[14] S.H. Baek, J. Park, D.M. Kim, V.A. Aksyuk, R.R. Das, S.D. Bu, D.A. Felker, J. Lettieri, V. Vaithyanathan, S.S.N. Bharadwaja, N. Bassiri-Gharb, Y.B. Chen, H.P. Sun, C.M. Folkman, H.W. Jang, D.J. Kreft, S.K. Streiffer, R. Ramesh, X.Q. Pan, S. Trolier-McKinstry, D.G. Schlom, M.S. Rzchowski, R.H. Blick, C.B. Eom, Giant Piezoelectricity on Si for Hyperactive MEMS, Science 334 (2011) 958–961.

[15] W. Wang, Q.X. Zhu, X.M. Li, M.M. Yang, X.D. Gao, X.Q. Zhao, Effects of ferroelectric/metal interface on the electric properties of PMN-PT thin films epitaxially grown on Si substrates, J Mater Sci: Mater Electron 24 (2013) 3782–3787.

[16] W.S. Tsang, K.Y. Chan, C.L. Mak, K.H. Wong, Spectroscopic ellipsometry study of epitaxially grown $Pb(Mg_{1/3}Nb_{2/3})O_3$-$PbTiO_3$/MgO/TiN/Si heterostructures, Appl. Phys. Lett. 83 (2003) 1599–1601.

[17] A. Lin, X. Hong, V. Wood, A.A. Verevkin, C.H. Ahn, R.A. McKee, F.J. Walker, E.D. Specht, Epitaxial growth of $Pb(Zr_{0.2}Ti_{0.8})O_3$ on Si and its nanoscale piezoelectric properties, Appl. Phys. Lett. 78 (2001) 2034–2036.

[18] S. Matsubara, N. Shohata, M. Mikami, Epitaxial Growth of $PbTiO_3$ on $MgAl_2O_4$/Si Substrates, Jpn. J. Appl. Phys. 24 (1985) 10–12.

[19] T. Arai, T. Ohno, T. Matsuda, N. Sakamoto, N. Wakiya, H. Suzuki, Effects of synthesis conditions on electrical properties of chemical solution deposition-derived $Pb(Mg_{1/3}Nb_{2/3})O_3$-$PbTiO_3$ thin films, Thin Solid Films 585 (2015) 86–90.

[20] J.H. Ma, X.J. Meng, J.L. Sun, T.Lin, F.W. Shi, G.S. Wang, J.H. Chu, Effect of excess Pb on crystallinity and ferroelectric properties of PZT(40/60) films on $LaNiO_3$ coated Si substrates by MOD technique, Applied Surface Science 240 (2005) 275–279.

[21] Y.C. Zhang, Z.Z. Yang, W.N. Ye, C.J. Lu, L.H. Xia, Effect of excess Pb on microstructures and electrical properties of $0.67Pb(Mg_{1/3}Nb_{2/3})O_3$–$0.33\ PbTiO_3$ ceramics, Mater Electron 22 (2011) 309–314.

[22] S.L. Swartz, T.R. Shrout, Fabrication of perovskite lead magnesium niobate, Mater. Res. Bull. 17 (1982) 1245.

[23] J. Jiang, S.-G. Hur, S.-G. Yoon, Electrical Properties of Epitaxial 0.65Pb($Mg_{1/3}Nb_{2/3}$)O_3-035$PbTiO_3$ Thin Films Grown on Buffered Si substrates by Pulsed Laser Deposition, Int. J. Appl. Ceram. Technol. 8 (2011) 1393–1399.

[24] J.-P. Maria, W. Hackenberger, S. Trolier-McKinstry, Phase development and electrical property analysis of pulsed laser deposited Pb($Mg_{1/3}Nb_{2/3}$)O_3-$PbTiO_3$ (70/30) epitaxial thin films, J. Appl. Phys. 84 (1998) 5147–5154.

[25] X.L. Zhong, L. Lu, M.O. Lai, Growth of highly orientated 0.65Pb($Mg_{1/3}Nb_{2/3}$)O_3–0.35$PbTiO_3$ films by pulsed laser deposition, Surface & Coatings Technology 198 (2005) 400–405.

[26] C. Pollak, B. Malic, M. Kosec, S. Javoric, H. Hutter, Chemical solution-deposited $PbZr_{0.53}Ti_{0.47}O_3$ on $La_{0.5}Sr_{0.5}CoO_3$. SIMS investigation of the effect of different precursor additives on the layer structure, Anal. Bioanal. Chem. 374 (2002) 608–613.

[27] J.H. Lee, M.R. Choi, W. Jo, J.Y. Jang, M.Y. Kim, Structural properties of 0.65Pb($Mg_{1/3}Nb_{2/3}$)O_3– 0.35$PbTiO_3$ relaxor ferroelectric thin films on $SrRuO_3$ conducting oxides, Ultramicroscopy 108 (2008) 1106–1109.

[28] S. Yokoyama, S. Okamoto, H. Funakubo, T. Iijima, K. Saito, H. Okino, T. Yamamoto, K. Nishida, T. Katoda, J. Sakai, Crystal structure, electrical properties, and mechanical response of (100)-/(001)-oriented epitaxial $Pb(Mg_{1/3}Nb_{2/3})O_3$-$PbTiO_3$ films grown on $(100)_cSrRuO_3$||$(100)SrTiO_3$ substrates by metal-organic chemical vapor deposition, J. Appl. Phys. 100 (2006) 054110.

[29] N.J. Donnelly, G. Catalan, C. Morros, R.M. Bowman, J.M. Gregg, Dielectric and electromechanical properties of $Pb(Mg_{1/3}Nb_{2/3})O_3$-$PbTiO_3$ thin films grown by pulsed laser deposition, J. Appl. Phys. 93 (2003) 9924–9929.

[30] H. Uršič, M.S. Zarnik, J. Tellier, M. Hrovat, J. Holc, M. Kosec, The influence of thermal stresses on the phase composition of $0.65Pb(Mg_{1/3}Nb_{2/3})O_3 – 0.35PbTiO_3$ thick films, J. Appl. Phys. 109 (2011) 014101.

[31] G. Catalan, M.H. Corbett, R.M. Bowman, J.M. Gregg, Effect of thermal expansion mismatch on the dielectric peak temperature of thin film relaxors, J. Appl. Phys. 91 (2002) 2295–2301.

[32] G. Vasta, T.J. Jackson, A. Frommhold, J. Bowen, E.J. Tarte, Residual stress analysis of all perovskite oxide cantilevers, J. Electroceram. 27 (2011) 176–188.

[33] F.S. Aguirre-Tostado, A. Herrera-Gómez, J.C. Woicik, R. Droopad, Z. Yu, D.G. Schlom, P. Zschack, E. Karapetrova, P. Pianetta, C.S. Hellberg, Elastic anomaly for SrTiO3 thin films grown on Si(001), Phys. Rev. B 70 (2004) 201403.

[34] G. Han, J. Ryu, W.-H. Yoon, J.-J. Choi, B.-D. Hahn, J.-W. Kim, D.-S. Park, C.W. Ahn, S. Priya, and D.-Y. Jeong, Stress-controlled $Pb(Zr_{0.53}Ti_{0.48})O_3$ thick films by thermal expansion mismatch between substrate and $Pb(Zr_{0.53}Ti_{0.48})O_3$ film, J. Appl. Phys. 110 (2011) 124101

[35] S. Nagakari, K. Kamigaki, S. Nambu, Dielectric Properties of Sol-gel Derived $Pb(Mg_{1/3}Nb_{2/3})O_3$-$PbTiO_3$ Thin Films, Jpn. J. Appl. Phys. 35 (1996) 4933–4935.

[36] S.D. Bu, M.K. Lee, C.B. Eom, W. Tian, X.Q. Pan, S.K. Streiffer, J.J. Krajewski, Perovskite phase stabilization in epitaxial $Pb(Mg_{1/3}Nb_{2/3})O_3$-$PbTiO_3$ films by deposition onto vicinal (001) $SrTiO_3$ substrates, Appl. Phys. Lett. 79 (2001) 3482–3484.

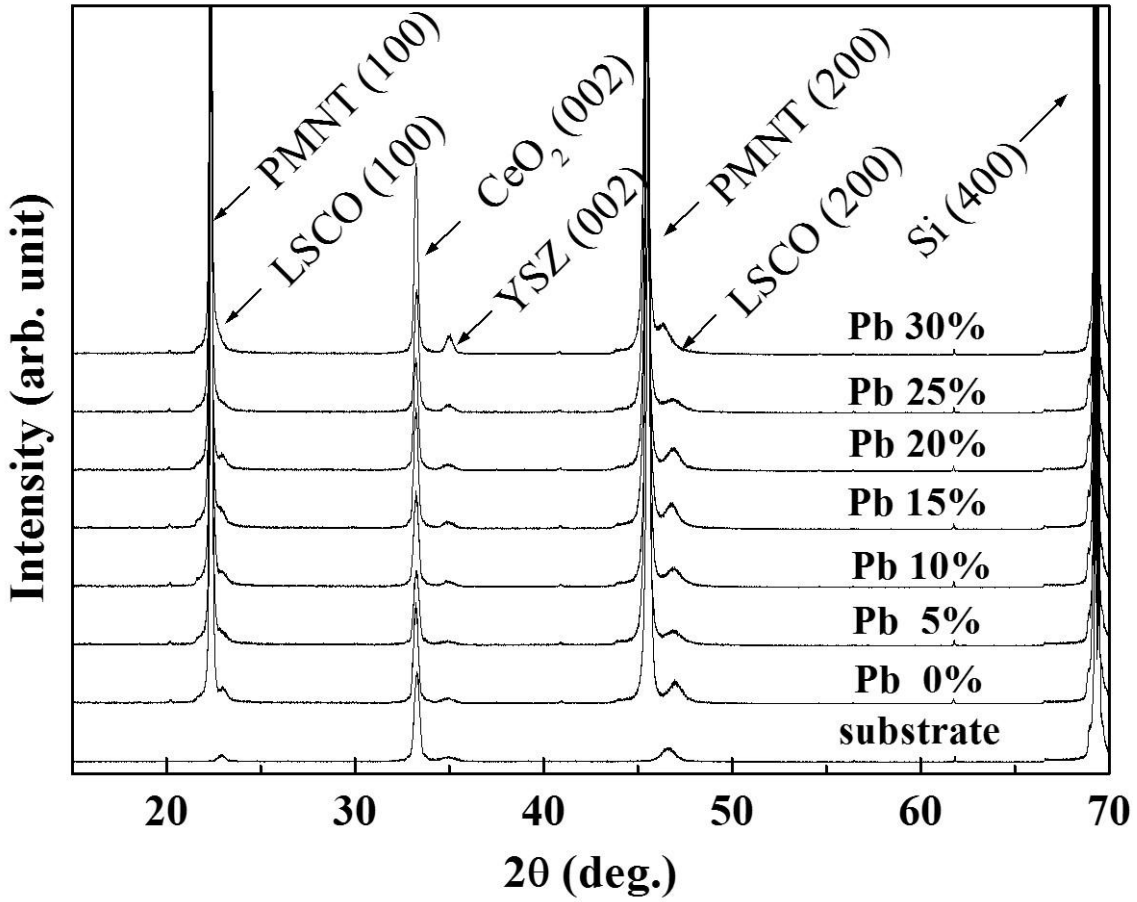

Figure 1

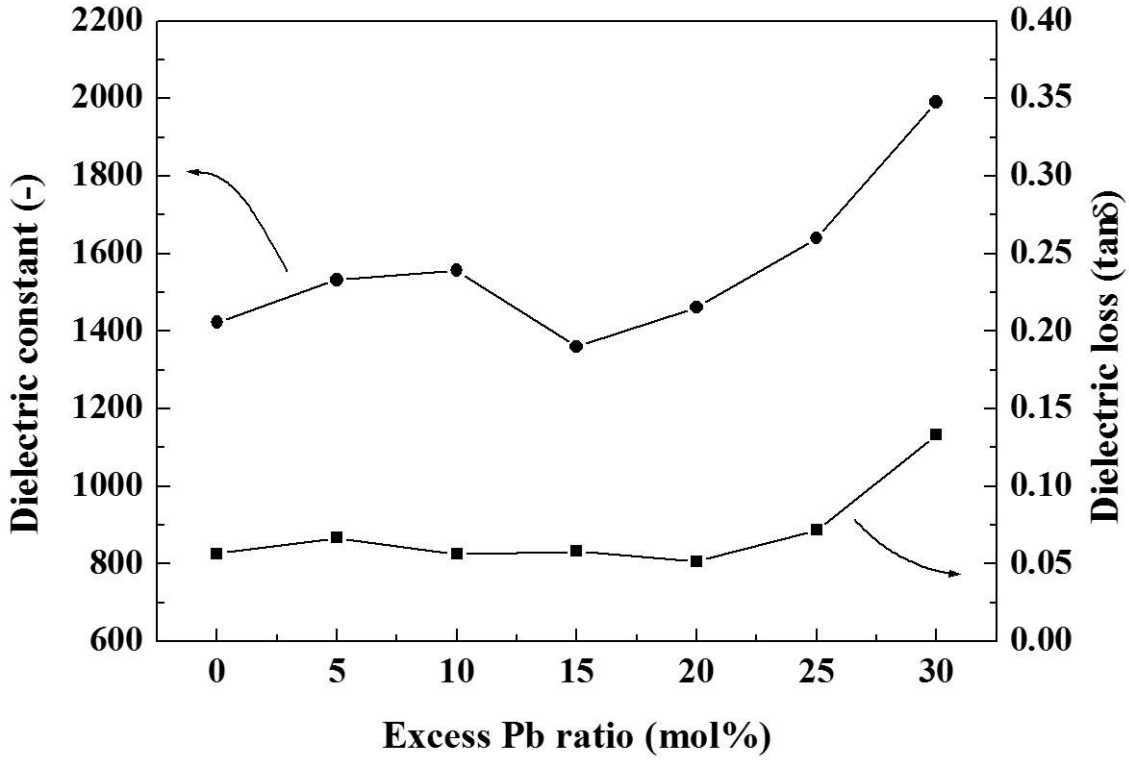

Figure 2

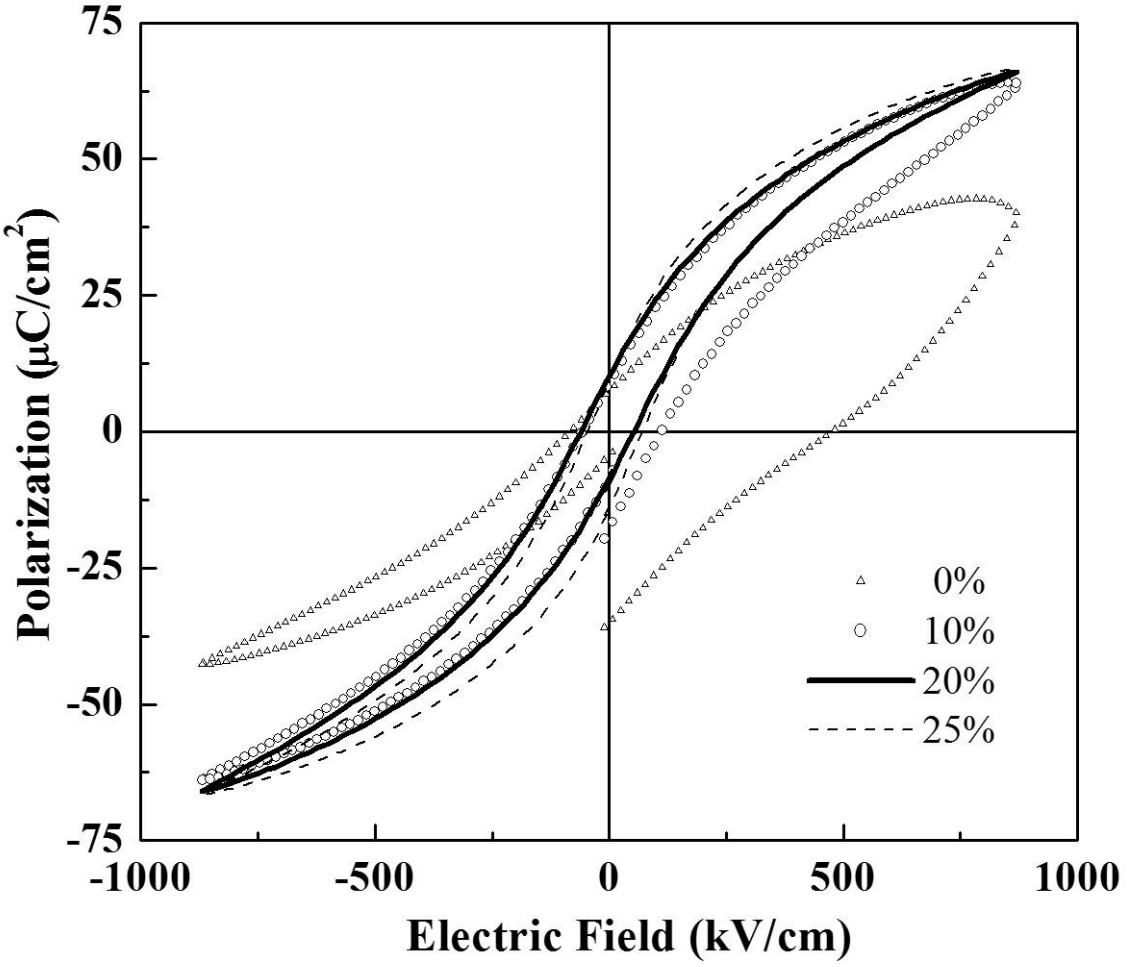

Figure 3

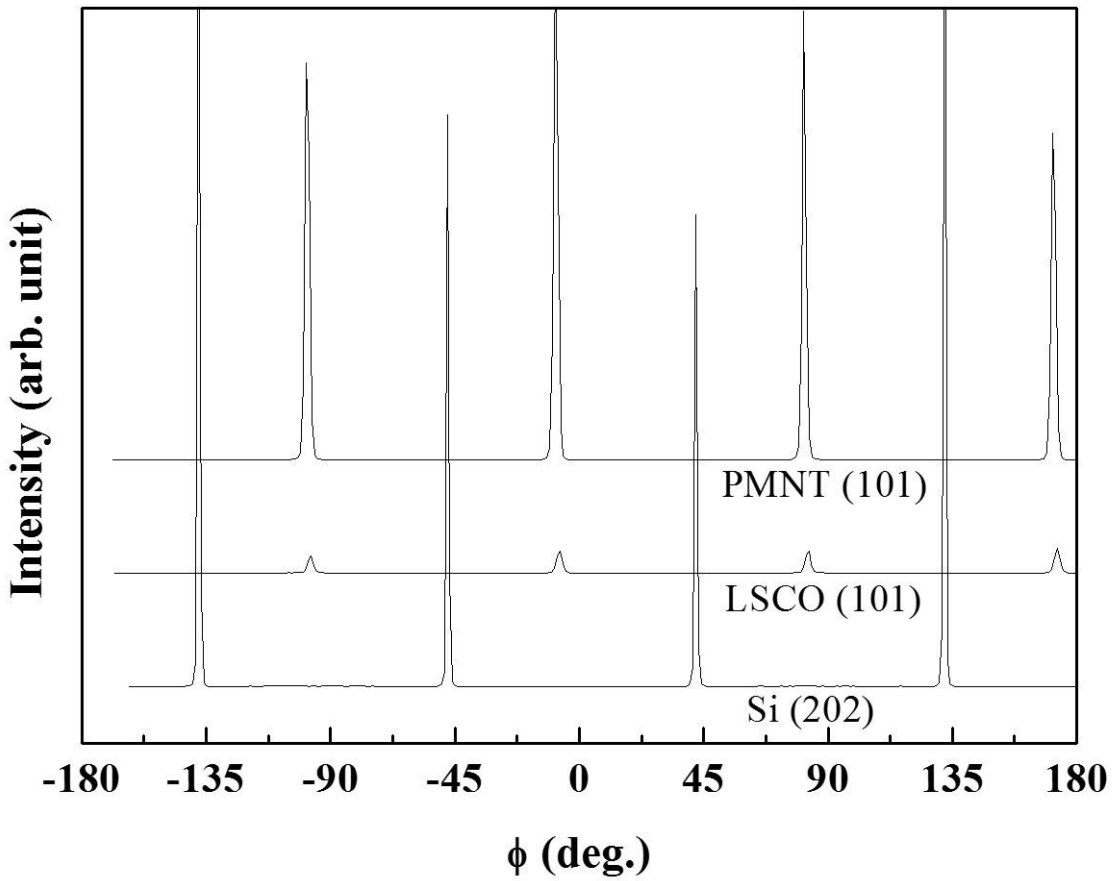

Figure 4

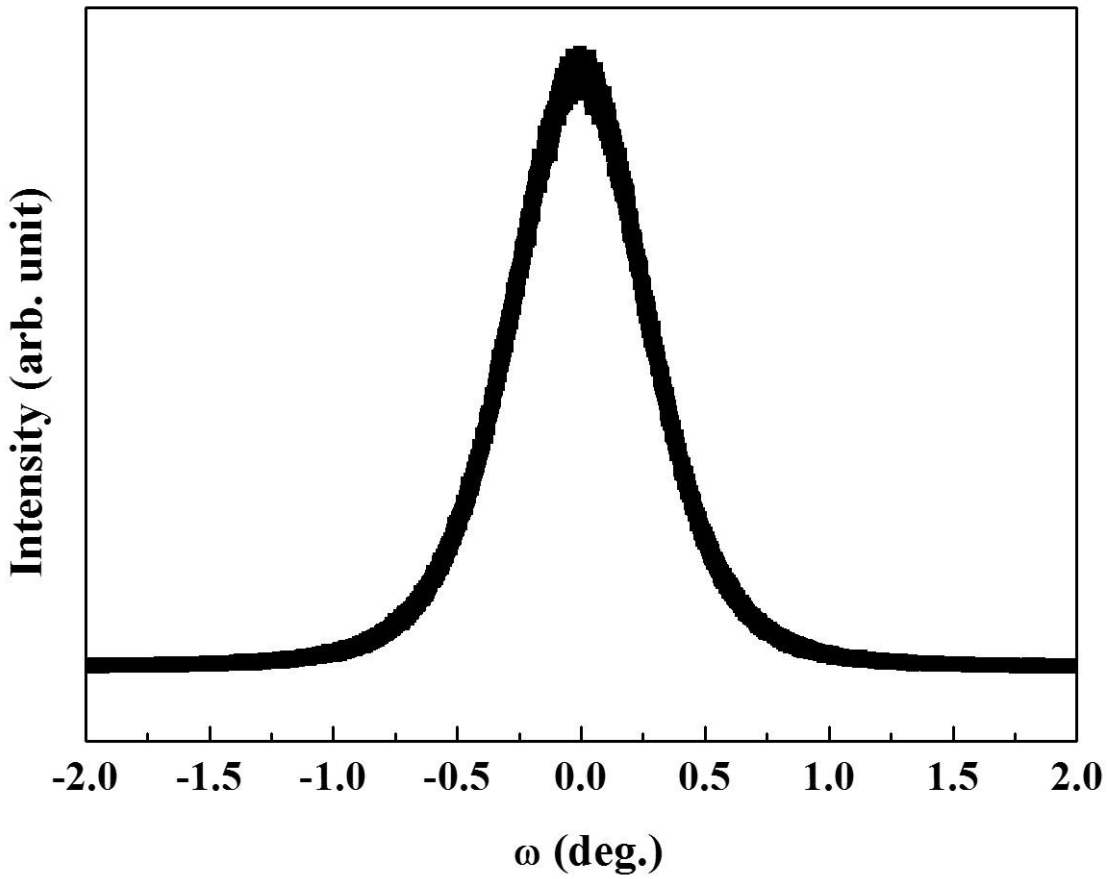

Figure 5

A

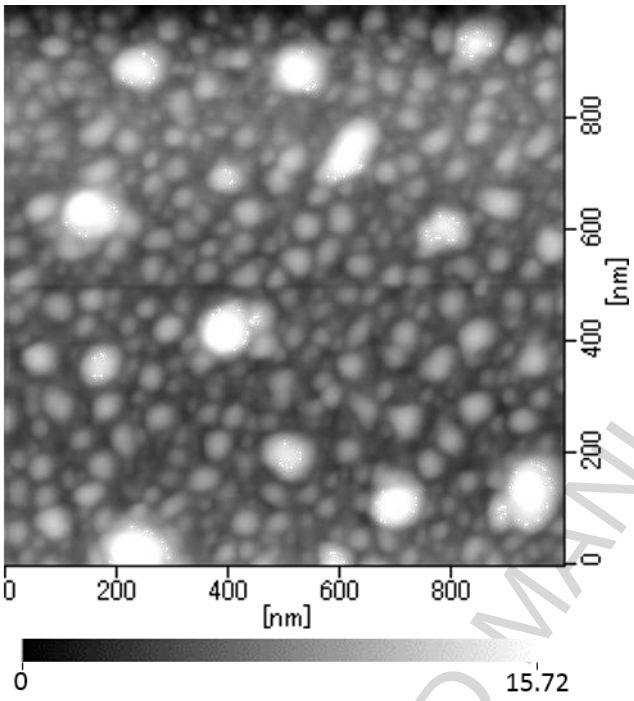

B

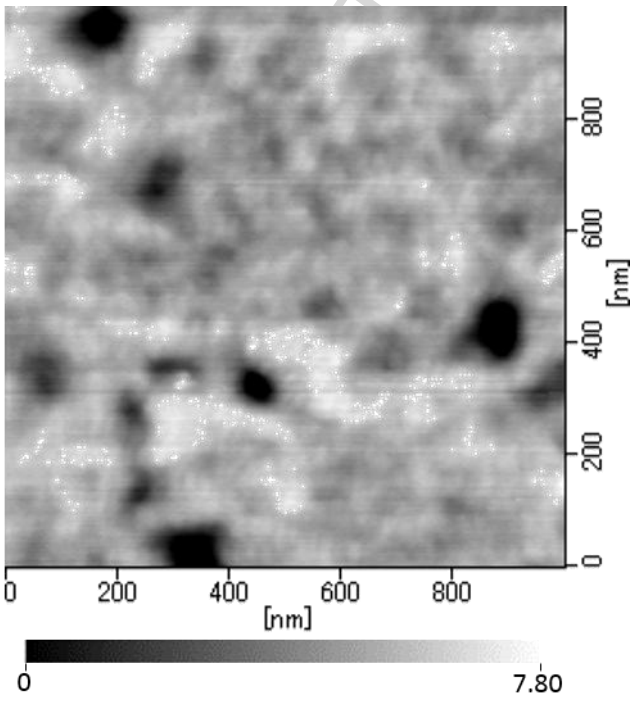

Figure 6

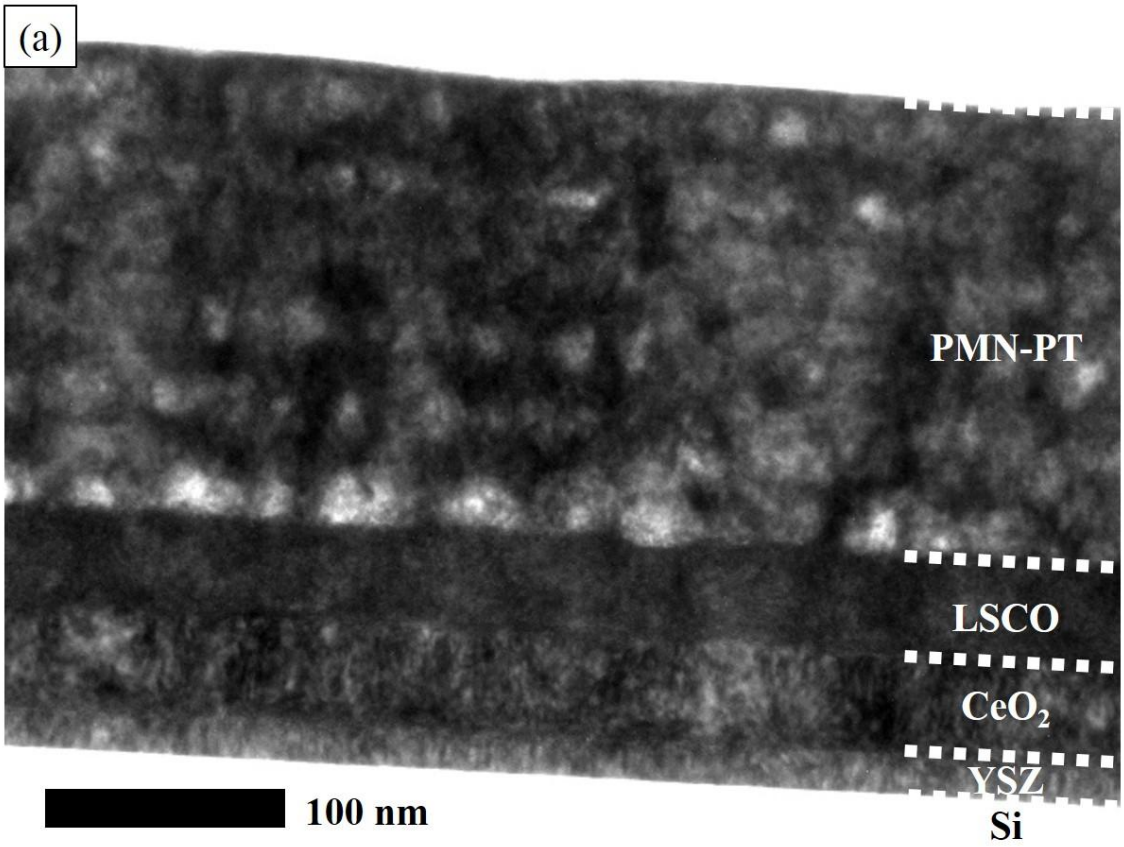

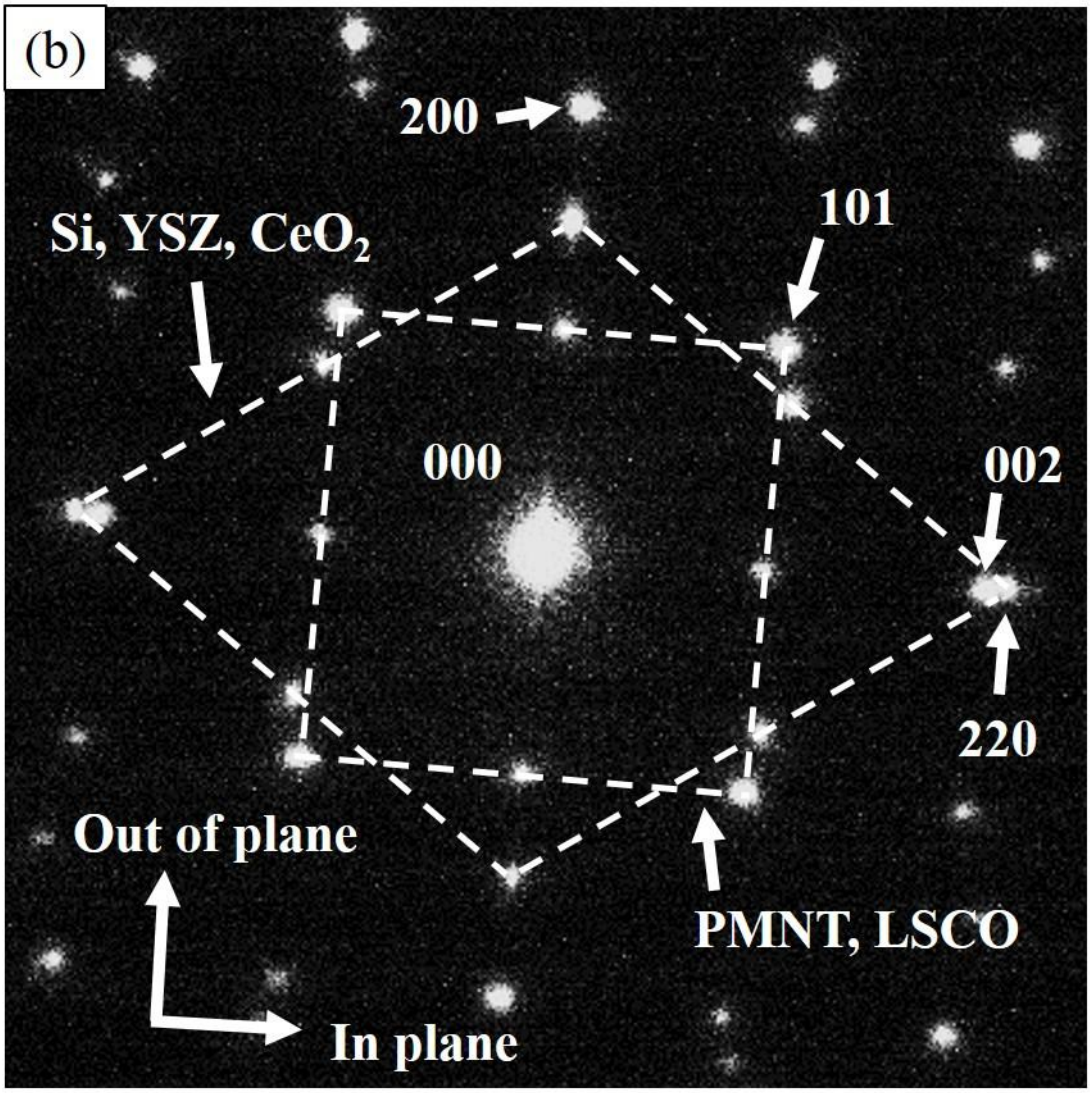

Figure 7

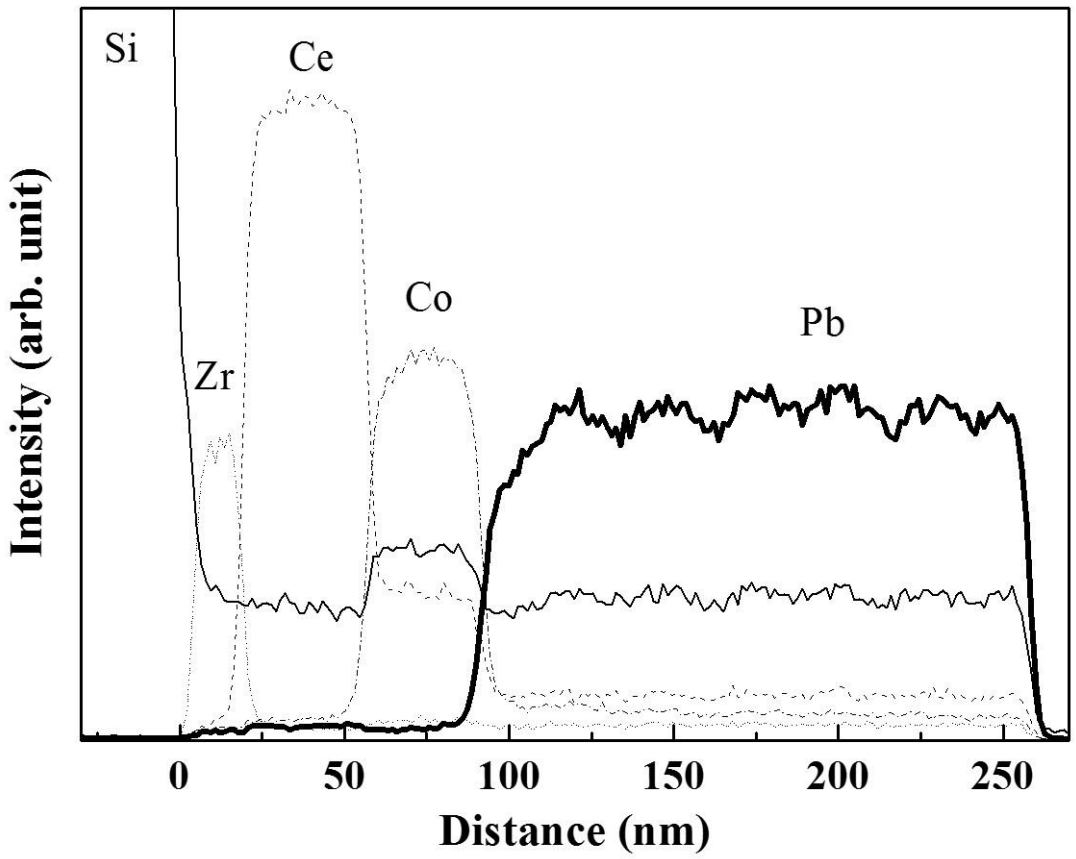

Figure 8

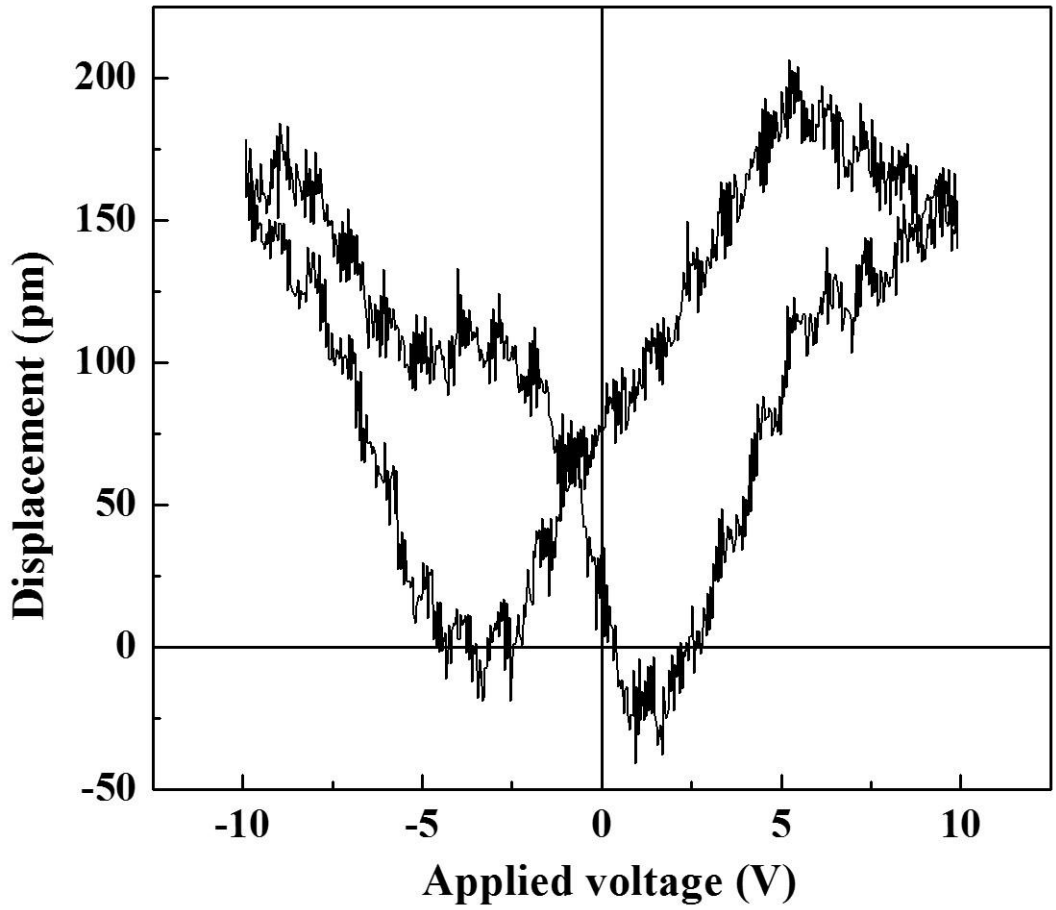

Figure 9

Table 1

composition	substrate structure	Pr (μC/cm)	ε	d33eff (pm/V))	Thickness (nm)	growth temp. (oC)	method	epitaxial	reference
65/35	Porous-LaNiO3/Si	27.7	4000	210	600	650	CSD		Our previous study [19]
67.5/32.5	LaNiO3/Si	7.5	2194	-	500	800	CSD		[3]
65/35	Pt/r-sapphire	-	2400	-	500	840	CSD		[35]
65/35	SrRuO3/SrTiO3	-	-	125	400	850	CSD	○	[27]
67/33	SrRuO3/SrTiO3	20	1000	-	-	600	Sputtering	○	[36]
70/30	LaNiO3/Pt/Si	7.44		65	600	450	Sputtering		[9]
65/35	SrRuO3/SrTiO3			120	2000–3000	650	CVD	○	[28]
70/30	SrRuO3/LaAlO3	20	1500	-	-	600	PLD	○	[24]
70/30	LSCO/MgO	(20)	(700)	(120)	500–1000	660	PLD		[29]
65/35	LaNiO3/LaAlO3	10.8	-	-	-	600–700	PLD	○	[25]
72/28	SrRuO3/SrTiO3/TiN/Si	15	1645		700	560	PLD	○	[15]
65/35	LSCO/CeO2/YSZ/Si	6.34	1631	-	300	550	PLD	○	[23]
65/35	LSCO/CeO2/YSZ/Si	9.1	1438	20	170	650	CSD	○	This study

Highlights

- $Pb(Mg_{1/3}Nb_{2/3})O_3$-$PbTiO_3$ (PMN-PT) epitaxial thin films were obtained on a Si wafer.
- Optimized Pb content in the precursor solution enhanced the electrical properties.
- Despite its 170-nm thickness, the PMN-PT thin film showed a permittivity of 1400.
- The 0.65PMN-0.35PT thin film showed a piezoelectric constant of 20 pm/V.